A multi-scale homogenization-based approach for dynamic simulation of lattice metamaterials

A multi-scale homogenization-based approach for dynamic simulation of lattice metamaterials

L. Cibrario [1], **C. Gastaldi** [1], **I. F. Cozza** [2], **G. Credo** [2], **M. Saracino** [2], **C. Delprete** [1], **F. Scarpa** [3]
[1] Politecnico di Torino, Department of Mechanical and Aerospace Engineering,
Corso Duca degli Abruzzi, 24, 10129, Turin, Italy
e-mail: **luca.cibrario@polito.it**

[2] Dumarey Automotive Italia S.p.A
Corso Castelfidardo, 36, 10129, Turin, Italy

[3] University of Bristol, Department of Aerospace Engineering,
Beacon House, Queens Rd, BS8 1QU, Bristol, United Kingdom

Abstract
Recent advancements in Additive Manufacturing have revolutionized mechanical component design. Lattice metamaterials, thanks to the possibility for effective control over their properties through the tuning of geometry layout, have gained great attention. However, the high computation time, required in all phases of numeric analyses is still a major challenge. The homogenization-based multi-scale analysis is a computationally efficient numerical approach, able to extrapolate the macroscopic behavior from microscopic analyses of unit cells. While homogenization techniques have been widely successful in static simulations, research on their dynamic behavior is still limited. Starting from the existing research in literature on composites, this study focuses on the development of a procedure based on the strain energy approach to retrieve the homogenized elastic and damping properties of lattice metamaterials. Moreover, the validity of the proposed algorithm is tested on a composite benchmark case and then applied to strut and surface-based lattices.

1 Introduction

In recent years, Additive Manufacturing (AM) has emerged a revolutionizing technology, enabling the production of complex shapes, that were once considered impossible to be manufactured through traditional processes. Among these developments, lattice structures have gained significant attention for their combination of strength, low weight, and highly customizable geometries [1]. Lattice structures are also known as metamaterials, being their macroscopic properties dependent on the geometric layout. This allows their behavior to be tailored on the application they are designed for, and, therefore, they can be employed in a really wide range of applications, including lightweight structures [2], heat exchangers, [3], energy absorbers [4], acoustic insulators [5, 6, 7] and in biomedical applications [8].

Lattice structures are systems of vertices connected with each other by beams or surfaces in repeatable sections, which form a single domain with a complex internal geometry. Therefore, they are topological ordered structures, formed by one or more repeating unit cells spatial arrangements with edges and faces formed by plates and struts. Cellular materials can have a wide range of topological features, length scales and structurally controlled characteristics. Lattice metamaterials are generally categorized into open-cell or close-cell, depending on the morphology and inter-connectivity of their unit cells. Another classification of is based on the level of randomness of the RVE, that leads to two main geometric behaviors: periodic and stochastic. Among the periodic category, lattice structures can be further differentiated based on their arrangement of unit cells: they can be beam (strut)-based or surface-based.

In strut-based unit cells, the connectivity of the struts, that is the number of beams linked at a given node,

greatly controls the structure behavior. For low or high connectivity, unit cells exhibit what is known as bending or stretch-dominated behavior, respectively [9, 10]. On the other hand, the most common types of surface-based unit cells are the triply periodic minimal surfaces (TPMS). They are a relatively new class of bio-inspired cellular materials, being investigated for their excellent convective thermal transport characteristics, and are mathematically defined surfaces, that exhibit minimum possible surface area within specified boundaries and zero mean curvature. The TPMS divides a given volume into two congruent regions: closing one of these volume gives a solid network, whereas the thickening of the TPMS gives a sheet network. TPMS-based geometries also have smooth profile, that eliminates the stress concentrations generated at the junctions of strut-based topologies and makes them self-supporting in the manufacturing phase [11, 3].

The easiest and most applied method to define mathematically a TPMS is a level-set approximation equation derived from a sum defined in terms of the Fourier series [12]:

$$\Psi(\mathbf{r}) = \sum_{\mathbf{k}} F(\mathbf{k}) \cos[2\pi \mathbf{k} \cdot \mathbf{r} - \alpha(\mathbf{k})] = 0 \tag{1}$$

where $\mathbf{k}$ is the reciprocal vector, $\alpha(\mathbf{k})$ is the phase shift and $F(\mathbf{k})$ is the structure factor, which is an amplitude associated to the $\mathbf{k}$ vector. Truncating the series to the leading term gives rise to a function, f that consists of a combination of trigonometric functions and satisfies the equality:

$$f(x, y, z) = c \tag{2}$$

Therefore, the function f defines a surface evaluated at the isovalue c and has a topology similar to that of a minimal surface. Two or more surfaces can also be plotted together as they do not intersect: two surfaces corresponding to two level-set constants with the same magnitude, but different signs have the same offset but in opposite directions from a hypothetical surface evaluated at the average of the two level-set values. When $c = 0$ the minimal surface thickness is 0, it does not have volume and the space is divided into two equal parts, while when $c \neq 0$ the isosurfaces are divided by a distance $2c$ and, if this space is filled, a solid minimal surface is generated. Fig. 1 depicts the most famous and used TPMS unit cells: Shoen gyroid, Schwartz primitive, Schwartz diamond, Shoen I-WP, Shoen F-RD, Neovius.

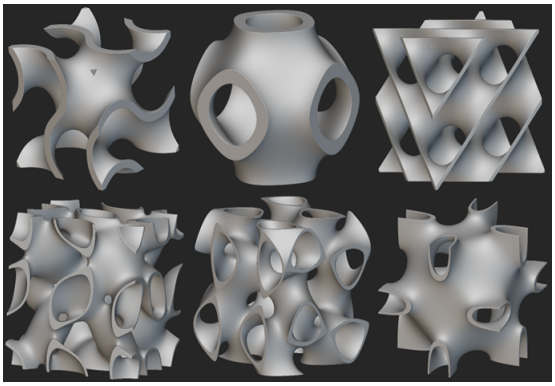

Figure 1: Examples of TPMS unit cells

Even if Finite Elements Method (FEM) and topology optimization (TO) are well-established and powerful tools for the mechanical design of lattice metamaterials, however, numerical analyses are usually unfeasible. In fact, a high computation time is needed for the simulation of even small components, due to the high number of mesh elements required to accurately model their complex geometry [2]. In this context, the multi-scale approach has emerged as a promising method to speed simulations up. It is based on homogenization, a numerical procedure that provides the mechanical properties in the micro-scale of the smallest domain able to reflect the behavior of the whole metamaterial, that is called Representative Volume Element (RVE). The equivalent mechanical properties can be used to model and simulate the whole lattice in the macro-scale as a bulk material, allowing the generation of lighter meshes and, therefore, leading to a huge saving in computation time [13]. Homogenization was originally introduced for composites materials and several procedures have been developed since the end of the 20^{th} century, ranging from analytical to numerical

approaches. A comprehensive overview of homogenization algorithms can be found in Barbero [14] and Somnic et al. [15].

Homogenization procedures based on numerical FE simulation are founded on the satisfaction of Hill-Mandel's theorem, that ensures the energetic consistency between the real and homogenized micro-scale models. From this requirement, three types of boundary conditions (BCs) can be employed to retrieve the equivalent mechanical properties: uniform boundary conditions (UBC) [16] either in form of traction or displacements, periodic boundary conditions (PBC) and enforced periodic boundary conditions (e-PBC), that are a combination of UBCs and PBCs [17]. Thus, several different algorithms originally developed for the homogenization of composite materials can be found in literature regarding the implementation of UBCs [18, 19], PBCs [20, 21] and e-PBCs [14].

While homogenization techniques have been widely successful in static simulations of lattice structures [22, 23], research on their dynamic behavior is still limited. Few studies in the literature have focused on the multi-scale dynamic analysis of composite materials, developing dynamic homogenization procedures in both the time and frequency domains, that involve coupled static-dynamic simulations and analysis of wave dispersion within the RVE [24, 25, 26, 27]. Their aim is the computation of the homogenized stiffness and damping properties, facilitating fast dynamic FEA of macro-scale components. Recently, homogenization has also been applied to lattice metamaterials to evaluate their mechanical properties and develop fast performing TO frameworks. However, the investigations conducted on lattice structures so far, have only concentrated on static loading cases and there is no trace in literature of a systematic procedure to perform multi-scale dynamic analyses of lattice structures relying on the homogenization procedure for structural application.

Taking inspiration from the above-mentioned existing literature on composites, this study focuses on the development of a reliable dynamic homogenization procedure and on its application on lattice metamaterials under the linearity hypothesis. The methodologies presented in this works are time-domain-based and two main approaches have been implemented, tested and compared on case studies: a simpler static algorithm that allows to retrieve the damping parameters through static numerical simulations, and the fully dynamic homogenization procedure [25], both based on the strain energy method [24]. The aim is to provide a complete workflow for the dynamic homogenization of lattice structures, comparing the strength, drawbacks and further capabilities of both the approaches. The authors also wanted to assess the validity of the dynamic implementation, even though it was proven to be much slower than the static one, because it allows multi-physics coupling. In fact, the final goal of the ongoing research will be the dynamic homogenization of lattices, accounting for fluid-structure interaction (FSI).

In the first section, the basis of homogenization are presented as long as the implementation of its dynamic versions, relying on an alternative and simpler approach to the commonly used periodic boundary conditions (PBCs), that was proposed by Steven [19, 18] for the static homogenization. Afterwards, the elasticity tensor and loss factors of both a strut-based and a TPMS lattice RVE are homogenized using the proposed algorithms. In section 2 the new formulation of the dynamic homogenization algorithm without PBCs is tested on a benchmark case of a composite material. The third section contains a convergence study on mesh and RVE dimensions to compare the performances of the homogenization algorithm presented in this paper and those relying on PBCs. In section 4 the results of the homogenization of a TPMS lattice structure using both the the static and dynamic implementations are reported, while the last one contains concluding remarks and future perspective on the application of the presented methodology.

2 Dynamic Homogenization: Theory and Implementation

2.1 Homogenization fundamentals

Multi-scale modeling refers to an approach in which the mechanical response of the material is studied at one length scale, but the outcomes of the analysis are referent to several properties at another one [23]. Homogenization is a technique for evaluating the equivalent macro-scale properties of a complex metamaterial with a periodic structure and it can be either performed through experiments or virtual tests based on numerical

simulations. Being the FEA of a whole lattice structure high demanding and often unfeasible due to the high number of mesh elements, numerical homogenization techniques have been developed and proven to lead to huge time saving in the simulation of complex lattice structures composed of hundreds or even thousands of repeated unit cells [28].

The homogenization approach was born to model composites materials [21], but can be effectively used also for lattices: the dual fiber-matrix phase composition of composites is replaced with the solid and void phases in lattices. The final goal of the procedure is to transform a porous periodic lattice structure into an equivalent solid material with homogenized properties, that make it behave as if it were a true lattice domain [29]. A fundamental problem that has to be solved to homogenize a lattice material is the definition of the minimum sufficient representative volume, so that the boundary conditions effects are minimized. To address this issue the concept of RVE was introduced [30]. The RVE is a region much smaller than the whole lattice structure, it has got the same mechanical characteristics and behavior of the lattice and its properties do not depend on boundary conditions.

Sub-scale modeling is energetically consistent, only if the deformation energy at the macroscopic level is equal to the volume average of the micro-scale stress work: at any equilibrium state of the RVE characterized by the stress field σ and the strain field ε, the following equation must be satisfied [31]:

$$\bar{\sigma}_{ij}\bar{\varepsilon}_{ij} = \frac{1}{V_{RVE}} \int_V \sigma_{ij}\varepsilon_{ij}\,\mathrm{d}V \tag{3}$$

where $\bar{\sigma}$ and $\bar{\varepsilon}$ are the average stress and strain tensors, V_{RVE} is the total volume of the RVE and the indexes i, j represent the principal directions. The average stress and strain are defined as [32]:

$$\begin{aligned} \bar{\sigma}_{ij} &= \frac{1}{V_{RVE}} \int_V \sigma_{ij}\,dV \\ \bar{\varepsilon}_{ij} &= \frac{1}{V_{RVE}} \int_V \varepsilon_{ij}\,dV. \end{aligned} \tag{4}$$

2.2 The Strain Energy Method and the "Static" Dynamic Homogenization

The dynamic homogenization procedure presented in this work, relies on the widely used strain energy approach, that was first proposed by Ungar and Kerwin [33]: the loss factor of the mechanical system can be expressed as the summation of the products of the individual element loss factors and the fraction of the total strain energy stored in each element, divided by the total stored energy:

$$\bar{\eta} = \frac{\sum_{i=1}^{n} \eta_i W_i^S}{\sum_{i=1}^{n} W_i^S} \tag{5}$$

where $\bar{\eta}$ is the homogenized loss factor, η_i is the loss factor of the i^{th} element, W_i^S is the energy stored in the i^{th} element at the maximum displacement and n is the total number of elements.

The strain energy method in its original formulation does not include any inertial effect when computing the equivalent viscoelastic properties of the metamaterial, making the numerical computation static. This assumption can be considered valid when the excitation frequencies applied to the mechanical component are much lower than its natural frequencies.

The constituent viscoelastic material of the lattice structure can be modeled using the complex modulus:

$$E = E^*(1 + i\eta) \tag{6}$$

where, E^* is the storage modulus and η is the loss factor. Thus, the stiffness matrix is expressed through the complex quantity

$$[C(\omega)] = [C_R(\omega)] + i\,[C_I(\omega)] \tag{7}$$

where C_R and C_I are the real and imaginary part of the stiffness matrix, respectively. The ratio between the

real and imaginary part of the complex stress-strain tensor represents the material loss factor tensor:

$$[\eta] = \frac{[C_I(\omega)]}{[C_R(\omega)]} \tag{8}$$

The determination of the effective mechanical properties of the lattice metamaterial implies the application of particular loading conditions to the RVE, that induce an overall deformation state in only one direction of the strain at a time.

Recalling, the Hooke's law, stress $\{\sigma\}$ and deformation $\{\varepsilon\}$ vectors are linked through the elasticity matrix $[E]$:

$$\{\sigma\} = [E]\{\varepsilon\} \tag{9}$$

Starting from the Hill-Mandel principle (Eq. 3), written in matrix form

$$\{\bar{\varepsilon}\}^T\{\bar{\sigma}\} = \frac{1}{V}\int_V \{\varepsilon\}^T\{\sigma\}\,\mathrm{d}V, \tag{10}$$

introducing Eq. 9 into Eq. 10, the first term can be rewritten as

$$\{\bar{\varepsilon}\}^T\{\bar{\sigma}\} = \{\bar{\varepsilon}\}^T[\bar{E}]\{\bar{\varepsilon}\} \tag{11}$$

where $[\bar{E}]$ is the homogenized elasticity tensor, that is the output of the homogenization procedure. If an overall deformation state, in which all the strain components are null with except to one, is applied to the RVE, taking for example the first iteration of the procedure, whose deformation state is

$$\{\bar{\varepsilon}\} = \{\bar{\varepsilon}_{11},\ 0,\ 0,\ 0,\ 0,\ 0\}^T \tag{12}$$

and substituting Eq. 12 into Eq. 11, the first term of Eq. 10 can be rewritten as

$$\{\bar{\varepsilon}\}^T\{\bar{\sigma}\} = \bar{C}_{11}(\bar{\varepsilon}_{11})^2 \tag{13}$$

Combining Eqs. 10 and 13, the first component of the elasticity tensor can be computed through:

$$\bar{C}_{11} = \frac{\frac{1}{V}\int_V \{\varepsilon\}^T\{\sigma\}\,\mathrm{d}V}{(\bar{\varepsilon}_{11})^2} \tag{14}$$

Recalling that

$$\frac{1}{V}\int_V \{\varepsilon\}^T\{\sigma\}\,\mathrm{d}V = 2\,\bar{W}^S, \tag{15}$$

where $\bar{W}^S$ is the average energy density stored inside the RVE, $\bar{C}_{11}$ can be finally determined through:

$$\bar{C}_{11} = \frac{2\,\bar{W}^S}{(\varepsilon^0_{11})^2} \tag{16}$$

The following approach can be used to homogenize both elastic and viscoelastic materials: the application of a displacement field induces a deformation state and, consequently, to the storage of elastic energy inside the RVE. The strain energy density stored in each element of the FE model can be computed through:

$$W^S_i = \frac{1}{2}\{\varepsilon_i\}^T\{\sigma_i\} \tag{17}$$

where $\{\varepsilon_i\}$ and $\{\sigma_i\}$ are the strain and stress vectors of the ith element, respectively, and V_i is the i$^{\mathrm{th}}$ element volume. On the other hand, the dissipated energy density can be computed through

$$W^d_i = 2\pi\eta\,\{\varepsilon_i\}^T\{\sigma_i\} \tag{18}$$

The average stored and dissipated energy density inside the RVE can be finally computed using:

$$\begin{aligned} \bar{W}^S &= \frac{\sum_{i=1}^{n} W_i^S V_i}{V_{RVE}} \\ \bar{W}^d &= \frac{\sum_{i=1}^{n} W_i^d V_i}{V_{RVE}} \end{aligned} \tag{19}$$

The mean stored and dissipated energy densities are finally used to compute the entries of the homogenized elasticity and loss factor tensors. As it can be deduced from Eq. 18, the numerical computation can be performed assigning to the material only the real part of the complex modulus, and the contribution from the dissipative forces are consequently obtained through the scaling factor η.

The complete set of BCs and the strategies for each of the nine simulation cases, required to compute all the homogenized properties, are resumed in Tables 1 and 2, where L_x, L_y and L_z are the RVE dimensions along the three principal directions. The uniform displacement BCs are taken from the homogenization algorithm proposed by Steven [19, 18] and fitted to the strain energy method, while the strategies for the computation of the homogenized properties were introduced by Shashidhar et al. [34]. In that work the PBCs, that are commonly used for homogenization, were employed. Since they require a periodic mesh, they could be difficult to setup for complex geometries, like the TPMS lattice structures. Steven's algorithm, while providing results comparable to those obtained through PBCs, can be applied to a generic mesh and, therefore, the implementation of the whole algorithm is simpler and straightforward.

Table 1: Nodal displacement boundary conditions for the nine load cases

Displacement boundary conditions									
Node coordinates	**Case 1**	**Case 2**	**Case 3**	**Case 4**	**Case 5**	**Case 6**	**Case 7**	**Case 8**	**Case 9**
$x = -L_x/2$	$\varepsilon_x = 0$	$\varepsilon_x = 0$	$\varepsilon_x = 0$	$\varepsilon_y = 0$	$\varepsilon_x = 0$	$\varepsilon_z = 0$	$\varepsilon_x = 0$	$\varepsilon_x = 0$	$\varepsilon_x = 0$
$x = L_x/2$	$\varepsilon_x = 1$	$\varepsilon_x = 0$	$\varepsilon_x = 0$	$\varepsilon_y = 0.5$	$\varepsilon_x = 0$	$\varepsilon_z = 0.5$	$\varepsilon_x = 1$	$\varepsilon_x = 0$	$\varepsilon_x = 1$
$y = -L_y/2$	$\varepsilon_y = 0$	$\varepsilon_y = 0$	$\varepsilon_y = 0$	$\varepsilon_x = 0$	$\varepsilon_z = 0$	$\varepsilon_y = 0$	$\varepsilon_y = 0$	$\varepsilon_y = 0$	$\varepsilon_y = 0$
$y = L_y/2$	$\varepsilon_y = 0$	$\varepsilon_y = 1$	$\varepsilon_y = 0$	$\varepsilon_x = 0.5$	$\varepsilon_z = 0.5$	$\varepsilon_y = 0$	$\varepsilon_y = 1$	$\varepsilon_y = 1$	$\varepsilon_y = 0$
$z = -L_z/2$	$\varepsilon_z = 0$	$\varepsilon_z = 0$	$\varepsilon_z = 0$	$\varepsilon_z = 0$	$\varepsilon_y = 0$	$\varepsilon_x = 0$	$\varepsilon_z = 0$	$\varepsilon_z = 0$	$\varepsilon_z = 0$
$z = L_z/2$	$\varepsilon_z = 0$	$\varepsilon_z = 0$	$\varepsilon_z = 1$	$\varepsilon_z = 0$	$\varepsilon_y = 0.5$	$\varepsilon_x = 0.5$	$\varepsilon_z = 0$	$\varepsilon_z = 1$	$\varepsilon_z = 1$

Table 2: Strategies for calculation of effective properties

Computation of the homogenized properties			
Load Case	**Storage tensor**	**Damping tensor**	**Loss factor tensor**
Case 1	$\bar{C}_{11}^R = \bar{W}^S / \left(0.5\bar{\varepsilon}_{11}^2\right)$	$\bar{C}_{11}^I = \bar{W}^d / \left(0.5\bar{\varepsilon}_{11}^2\right)$	$\bar{\eta}_{11} = (1/2\pi)\bar{W}^S/\bar{W}^d$
Case 2	$\bar{C}_{22}^R = \bar{W}^S / \left(0.5\bar{\varepsilon}_{22}{}^2\right)$	$\bar{C}_{22}^I = \bar{W}^d / \left(0.5\bar{\varepsilon}_{22}{}^2\right)$	$\bar{\eta}_{22} = (1/2\pi)\bar{W}^S/\bar{W}^d$
Case 3	$\bar{C}_{33}^R = \bar{W}^S / \left(0.5\bar{\varepsilon}_{33}{}^2\right)$	$\bar{C}_{33}^I = \bar{W}^d / \left(0.5\bar{\varepsilon}_{33}{}^2\right)$	$\bar{\eta}_{33} = (1/2\pi)\bar{W}^S/\bar{W}^d$
Case 4	$\bar{C}_{44}^R = \bar{W}^S / \left(0.5\bar{\varepsilon}_{23}{}^2\right)$	$\bar{C}_{33}^I = \bar{W}^d / \left(0.5\bar{\varepsilon}_{33}{}^2\right)$	$\bar{\eta}_{44} = (1/2\pi)\bar{W}^S/\bar{W}^d$
Case 5	$\bar{C}_{55}^R = \bar{W}^S / \left(0.5\bar{\varepsilon}_{13}{}^2\right)$	$\bar{C}_{55}^I = \bar{W}^d / \left(0.5\bar{\varepsilon}_{13}{}^2\right)$	$\bar{\eta}_{55} = (1/2\pi)\bar{W}^S/\bar{W}^d$
Case 6	$\bar{C}_{66}^R = \bar{W}^S / \left(0.5\bar{\varepsilon}_{12}{}^2\right)$	$\bar{C}_{66}^I = \bar{W}^d / \left(0.5\bar{\varepsilon}_{12}{}^2\right)$	$\bar{\eta}_{66} = (1/2\pi)\bar{W}^S/\bar{W}^d$
Case 7	$\bar{C}_{12}^R = \bar{C}_{21}^R = U_{12}^R$	$\bar{C}_{12}^I = \bar{C}_{21}^I = U_{12}^I/2\pi$	$\bar{\eta}_{12} = (1/2\pi)\bar{W}^S/\bar{W}^d$
	$U_{12}^R = \bar{W}^S - 0.5\left(\bar{C}_{11}^R\bar{\varepsilon}_{11}^2 + \bar{C}_{22}^R\bar{\varepsilon}_{22}^2\right)$	$U_{12}^I = \bar{W}^d - \pi\left(\bar{C}_{11}^I\bar{\varepsilon}_{11}^2 + \bar{C}_{22}^I\bar{\varepsilon}_{22}^2\right)$	$\bar{\eta}_{21} = (1/2\pi)\bar{W}^S/\bar{W}^d$
Case 8	$\bar{C}_{23}^R = \bar{C}_{32}^R = U_{23}^R$	$\bar{C}_{23}^I = \bar{C}_{32}^I = U_{23}^I/2\pi$	$\bar{\eta}_{23} = (1/2\pi)\bar{W}^S/\bar{W}^d$
	$U_{23}^R = \bar{W}^S - 0.5\left(\bar{C}_{22}^R\bar{\varepsilon}_{22}^2 + \bar{C}_{33}^R\bar{\varepsilon}_{33}^2\right)$	$U_{23}^I = \bar{W}^d - \pi\left(\bar{C}_{22}^I\bar{\varepsilon}_{22}^2 + \bar{C}_{33}^I\bar{\varepsilon}_{33}^2\right)$	$\bar{\eta}_{32} = (1/2\pi)\bar{W}^S/\bar{W}^d$
Case 9	$\bar{C}_{13}^R = \bar{C}_{31}^R = U_{13}^R$	$\bar{C}_{13}^I = \bar{C}_{31}^I = U_{13}^I/2\pi$	$\bar{\eta}_{13} = (1/2\pi)\bar{W}^S/\bar{W}^d$
	$U_{13}^R = \bar{W}^S - 0.5\left(\bar{C}_{11}^R\bar{\varepsilon}_{11}^2 + \bar{C}_{33}^R\bar{\varepsilon}_{33}^2\right)$	$U_{13}^I = \bar{W}^d - \pi\left(\bar{C}_{11}^I\bar{\varepsilon}_{11}^2 + \bar{C}_{33}^I\bar{\varepsilon}_{33}^2\right)$	$\bar{\eta}_{31} = (1/2\pi)\bar{W}^S/\bar{W}^d$

2.3 Fully Dynamic Homogenization

The strain energy approach can be also employed in a fully dynamic implementation. In this case the homogenized elastic and viscoelastic properties are retrieved through the analysis of a complete vibration cycle at a desired excitation frequency $\bar{f}$. Instead of solving the static equilibrium equation, the dynamic equation of motion of the RVE is solved in the time domain:

$$[M]\{\ddot{q}\} + [C]\{\dot{q}\} + [K]\{q\} = \{F(t)\} \tag{20}$$

where $[M]$, $[C]$ and $[K]$ are the mass, damping and stiffness matrix of the mechanical system, respectively, $\{q\}$ is the vector of the coordinates of the degrees of freedom of the system and $\{F(t)\}$ is the external excitation.

Modeling the damping contribution of the viscoelastic properties of the base material through the Rayleigh's stiffness matrix-proportional coefficient β

$$[C] = \beta\,[K], \tag{21}$$

the correlation between β and the loss factor η would be:

$$\beta = \frac{\eta}{2\pi\bar{f}} \tag{22}$$

The dynamic homogenization is performed iteratively applying to the RVE the same BCs as in the static implementation (take Table 1 as reference). However, the exciting displacement BC is now in the form:

$$\varepsilon_{ij}(t) = \bar{\varepsilon}_{ij}\sin(2\pi\bar{f}\,t) \tag{23}$$

where $\bar{\varepsilon}_{ij}$ is maximum strain amplitude of the excitation.

In each iteration of the homogenization procedure a full loading cycle is simulated and it is divided in smaller time steps, in which the homogenized stress is computed. Recalling the expression for the average stress

$$\bar{\sigma}_{ij} = \frac{1}{V}\int_V \sigma_{ik}x_j n_k\,\mathrm{d}S, \tag{24}$$

since the stress distribution within the RVE must satisfy the periodicity condition, then two corresponding points on two opposite planes (with same in-plane coordinates) must have the same normal and shear stresses. Therefore:

$$\bar{\sigma}_{ij} = \frac{1}{v}\left(\int_{S_m^+}\sigma_{im}^+ x_j^+\,\mathrm{d}S - \sigma_{im}^- x_j^-\,\mathrm{d}S\right) = \frac{1}{v}\int_{S_m^+}\sigma_{im}^+(x_j^+ - x_j^-)\,\mathrm{d}S \tag{25}$$

In the above the suffix m is a dummy suffix. When $m \neq j$ the coordinates $x_j^+ = x_j^-$ and when $m = j$, $x_j^+ - x_j^- = \Delta x_j$, so

$$\bar{\sigma}_{ij} = \frac{\Delta x_j}{V}\int_{s_j}\sigma_{ij}\,\mathrm{d}S = \frac{F_{ij}}{S_j} \tag{26}$$

The above equation indicates that the average stresses can be simply obtained from the ratio between the resultant traction F_{ij} on the boundary surfaces and the areas of the corresponding boundary surfaces.

Therefore, at each time step of the dynamic simulation the force reaction F_{ij} can be computed and plotted against the displacement u_{ij} that is the average displacement in direction j of the RVE face with the maximum coordinate and normal along direction i. In this way, an hysteresis plot is obtained and its area corresponds to the total dissipated energy throughout the loading cycle, which is the product of the mean dissipated energy density and the volume of the RVE:

$$\bar{W}^d\,V_{RVE} = \int_{u_{ij,min}}^{u_{ij,max}} F_{ij}\,du_{ij} \tag{27}$$

The mean stored energy density can be computed through

$$\bar{W}^S = \frac{1}{2} F_{ij}^{max}\, u_{ij}^{max} \tag{28}$$

where F_{ij}^{max} and u_{ij}^{max} are the maximum reaction force and displacement values. At each iteration, after having obtained $\bar{W}^S$ and $\bar{W}^d$, the homogenized properties can again be computed as it is described in Table 2.

3 A first test case on composites: comparison with benchmark data

A preliminary investigation was performed on a glass fiber reinforced composite test case to compare the results from the homogenization presented in this paper to those found in literature. The simulation were performed on a RVE composed of a cylindrical inclusion inside a rectangular cuboid with dimensions 10 x 10 x 2 mm (Fig. 2). The fiber, that occupies the 30% of the total volume, and the matrix are isotropic viscoelastic materials with the following properties:

- Fiber: $E_f = 72.4$ GPa, $\nu_f = 0.2$, $\eta_f = 0.0018$
- Matrix; $E_m = 2.76$ GPa, $\nu_m = 0.35$, $\eta_m = 0.015$

Results were compared to those of Chandra et al. [24] and Conejos et al. [35], who employed the strain-energy approach in the static formulation, and Rezaei et al. [25], that first proposed the fully dynamic implementation with PBCs.

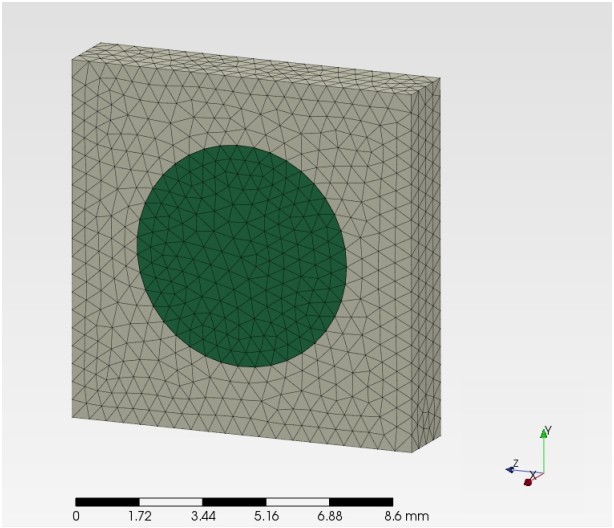

Figure 2: FE mesh of the composite RVE with cylindrical inclusion

The comparison of the results about the loss factors in the principal direction is summarized in Table 3, where SI and DI stand for the static implementation and the dynamic implementation of the dynamic homogenization presented in this study. As it can be seen, the results of are quite close those available in literature, with exception for the loss factor in the axial direction, that shows a slightly higher difference for both the version of the dynamic homogenization.

4 Convergence study of homogenization algorithms on a strut-based lattice RVE

In the previous section there is a proof of the validity of Steven's BCs with respect to the the widely famous PBCs. However, a more systematic comparative study in dependence of mesh and RVE size was performed

Table 3: Comparison of loss factors for a cylindrical inclusion for volume fiber of 30%

Loss factor comparison					
	Chandra [24]	Conejos [35]	Rezaei [25]	SI	DI
$\bar{\eta}_{11}$ [%]	0.31	0.30	0.28	0.35	0.35
$\bar{\eta}_{22}$ [%]	1.48	1.49	1.43	1.44	1.44
$\bar{\eta}_{12}$ [%]	1.48	1.49	1.46	1.47	1.47
$\bar{\eta}_{23}$ [%]	1.47	1.48	1.43	1.42	1.44

on a strut-based lattice structure and its outcomes are presented in this section. The goal was the evaluation of the best trade off between the accuracy of results and the computation time to retrieve the components of the real elasticity tensor. Steven's approach was compared to PBCs in two different formulations: the relative and absolute coupling. More information on the base theory and the way to implement them can be found in [14, 36, 21]. The lattice under test is composed of tetra strut-based unit cells, which is obtained combined a cubic and a BCC unit cell, with side length $L = 6$ mm and beam thickness $t = 0.75$ mm. The base material is the aluminum alloy AlSi10Mg, modeled as an isotropic material with the following properties: $E = 70$ Gpa, $\nu = 0.33$.

Strut-based and TPMS-based lattices can be modeled as orthotropic materials with cubic symmetry. Thus, the elastic constitutive law of the material can be described using only the three independent parameters: the in-plane elastic constant C_{11}, out-of-plane elastic constant C_{12} and shear component C_{44}. Therefore, the elasticity tensor is in the following form [37]:

$$[C] = \begin{bmatrix} C_{11} & C_{12} & C_{12} & 0 & 0 & 0 \\ C_{12} & C_{22} & C_{12} & 0 & 0 & 0 \\ C_{12} & C_{12} & C_{33} & 0 & 0 & 0 \\ 0 & 0 & 0 & C_{44} & 0 & 0 \\ 0 & 0 & 0 & 0 & C_{44} & 0 \\ 0 & 0 & 0 & 0 & 0 & C_{44} \end{bmatrix} \tag{29}$$

This allows the full characterization of the homogenized material performing only three out of the nine simulations, that correspond to cases 1, 4 and 7 presented in Tables 1 and 2.

The design of the RVE was performed using a totally free and open-source tool developed by the authors in Python and GNU Octave. The RVE was then meshed with quadratic tetrahedra using the free software Gmsh. The setup of the FE model as well as the post processing activities for each iteration of the homogenization procedure were performed using self-developed Python scripts able to create the input file for the FE open-source software CalculiX and analyze its output.

Fig. 3 reports the results of the convergence study on the components of the homogenized elasticity for an increasing number of elements per cell and for RVE composed of 1, 8 and 27 cells. As it can be clearly seen, Steven's approach provides barely the same results as PBCs, so it can be effectively used in homogenization frameworks. Moreover, for this RVE an convergence of the results is achieved after 30000 elements per unit cell and the number of unit cells in the RVE does not influence the outcomes.

5 Dynamic homogenization of a TPMS lattice structures

After having proved the validity of the proposed framework, in this section the effective mechanical properties of a TPMS lattice structure are homogenized using both the static and dynamic approach presented in section 2. The goal is the determination, after a convergence study, of the homogenized elastic and damping tensors of the metamaterial, that can be employed in further macro-scale static and dynamic analyses, to

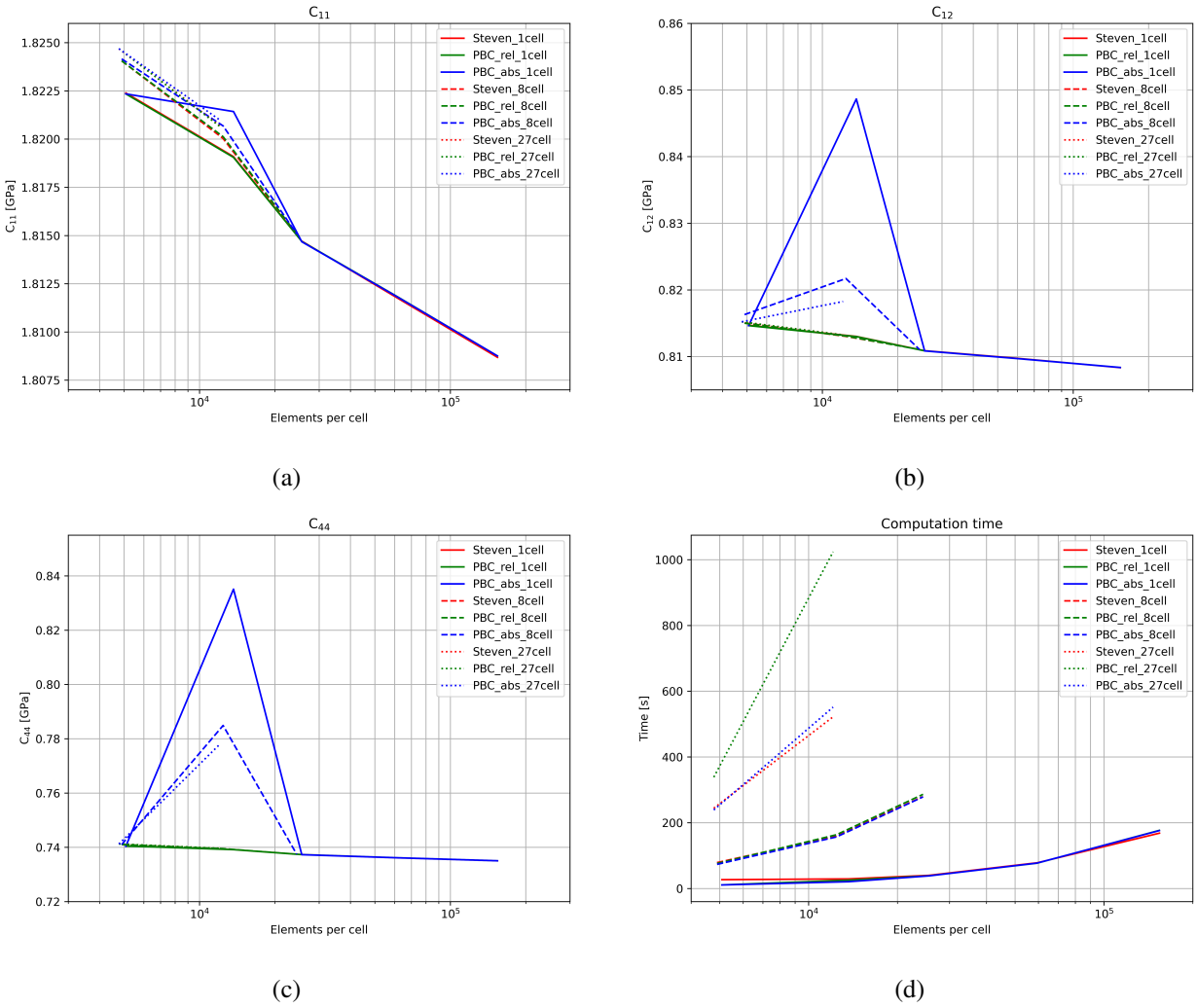

Figure 3: Results of the convergence study on the C_{11} (a), C_{21} (b), C_{44} (c) components of the homogenized elasticity tensor and overall computation time (d)

dramatically reduce the overall computation time. In this test case the RVE of a Schwartz primitive lattice is homogenized. This unit cell is mathematically defined as the solution to the following equation:

$$f(x, y, z) = \cos(x) + \cos(y) + \cos(z) = c \tag{30}$$

The unit cell was designed within a cubic domain with side length 10 mm, which is an average dimension of the most commonly used TPMS lattices for practical applications, and with 30% relative density. The base material of the RVE is steel with the following properties: $E = 210$ GPa, $\nu = 0.28$ and $\eta = 0.01$. The FE model of the lattice test case is represented in Fig. 4a.

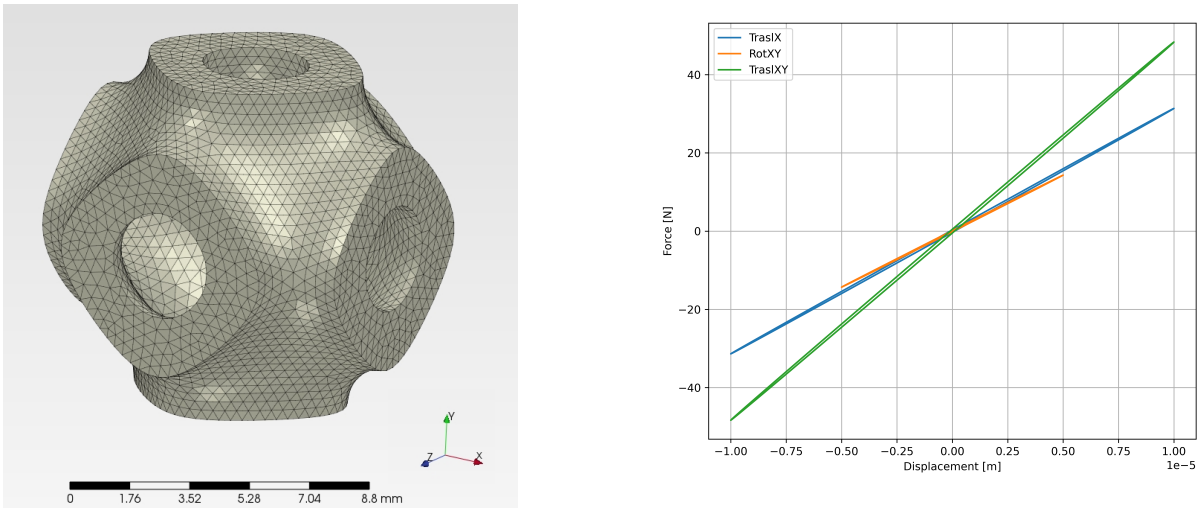

(a) (b)

Figure 4: FE model of the primitive unit cell (a) and Hysteresis cycles (b)

TPMS unit cells like the Schwartz primitive can be modeled as an orthotropic material with cubic symmetry and, as in the case of the strut-based lattice tested in the previous section, their mechanical behavior is fully characterized through C_{11}, C_{12} and C_{44}.

A preliminary modal analysis was performed on the RVE without any displacement constraint to assess the value of the first resonant frequency, not regarding free body motion, and check if the hypotheses for the validity of the static implementation of the dynamic implementation were valid. In fact, as presented in section 2.2, the homogenized properties, computed in this way, are valid only if the excitation frequency, applied to the macroscopic model, are far below the first resonant frequency, i.e. the inertial contribution can be neglected. It was checked that the first resonant frequency was around 87.5 kHz, that is much bigger than common mechanical vibration frequencies.

The dynamic approach was performed simulating a full sinusoidal loading cycle in each iteration with frequency $\bar{f} = 1$ Hz and maximum strain amplitude $\bar{\varepsilon}_{ij} = 0.001$. It should be noted that the maximum strain amplitude does not influence the results, since the linearity hypothesis holds.

From the numerical analyses it was found that the mesh size does not influence the results of the homogenized loss factor, as also reported in Conejos et al. [35], while it has effect on the components of both the real and imaginary parts of the complex stress–strain tensor. Convergence was found with an RVE of about 30000 quadratic tetrahedron mesh elements. Table 4 summarizes the data obtained through the two dynamic homogenization approaches and Fig. 4b depicts the hysteresis cycles for the three cases simulated in the dynamic algorithm.

As it can be seen from the results, both the dynamic homogenization algorithms provide almost the same effective mechanical properties. However the static implementation is much faster, but it has got the limitation to provide reliable data only for excitation frequencies that are far below the first resonant frequency of

Table 4: Homogenized mechanical properties and total computation time for the dynamic homogenization of the primitive RVE with 30% relative density

Homogenized properties		
Mechanical property	Static algorithm	Dynamic algorithm
$\bar{C}^S_{11}$ [GPa]	31.3	31.4
$\bar{C}^S_{12}$ [GPa]	16.9	16.7
$\bar{C}^S_{44}$ [GPa]	14.3	14.3
$\bar{C}^d_{11}$ [GPa]	0.313	0.314
$\bar{C}^d_{12}$ [GPa]	0.169	0.167
$\bar{C}^d_{44}$ [GPa]	0.143	0.143
$\bar{\eta}_{11}$ [%]	1.00	1.00
$\bar{\eta}_{12}$ [%]	1.00	1.00
$\bar{\eta}_{44}$ [%]	1.00	1.00
Time	30 s	15 min

the lattice. On the contrary, the fully dynamic algorithm, even though it is slower, gives complete freedom to simulate the behavior at any excitation frequency and can be also employed for the simulation of RVEs when non-linearities are present.

6 Conclusions

This work's aim was to provide a homogenization algorithm able to simulate the viscoelastic behavior of materials with complex micro-structure and provide their homogenized properties for multi-scale macroscopic analyses, in order to save computation time, that is still one of the major limitations in the FEM of lattice metamaterials.

Two main approaches of the dynamic homogenization, derived from the existing literature on composites and based on the strain energy approach, were presented. The former is performed through static FEA and it can be applied when the frequency of external excitation are much lower than the natural frequencies of the RVE. The latter consists in a fully dynamic algorithms able to retrieve the homogenized properties from the analysis of the hysteresis cycles. Both the implementations rely on the UBCs formulation presented in the work by Steven, and they were proven to provide comparable results to PBCs. Moreover, the presented framework was applied to a composite benchmark case and the results were promising.

Finally, both the algorithms were applied to a TPMS lattice structure, a kind of lattices with great potentials in many different fields of application and that have not yet been sufficiently analyzed due to the difficulties in numerical analyses and manufacturing. The dynamic homogenization of lattice structures does not provide additional information with respect to the static one, because the output homogenized loss factor coincides with that of the base material. That is quite obvious, since lattices are made just of a single material. However, the dynamic implementation seems to be a promising algorithm to homogenize mechanical systems with multi-physic and non-linear phenomena: TPMS lattices are becoming crucial for the design of advanced heat exchangers with far superior performances with respect to traditional ones, therefore, the analysis of the coupled fluid-structure behavior will be essential for their mechanical design.

References

[1] H. N. Wadley, "Multifunctional periodic cellular metals," *Philosophical Transactions of the Royal Society A: Mathematical, Physical and Engineering Sciences*, vol. 364, no. 1838, pp. 31–68, Dec.

2005. [Online]. Available: https://royalsocietypublishing.org/doi/10.1098/rsta.2005.1697

[2] J. Zhu, H. Zhou, C. Wang, L. Zhou, S. Yuan, and W. Zhang, "A review of topology optimization for additive manufacturing: Status and challenges," *Chinese Journal of Aeronautics*, vol. 34, no. 1, pp. 91–110, Jan. 2021. [Online]. Available: https://www.sciencedirect.com/science/article/pii/S1000936120304520

[3] K. Dutkowski, M. Kruzel, and K. Rokosz, "Review of the State-of-the-Art Uses of Minimal Surfaces in Heat Transfer," *Energies*, vol. 15, no. 21, 2022.

[4] M. Benedetti, p. u. family=Plessis, given=A., R. O. Ritchie, M. Dallago, S. M. J. Razavi, and F. Berto, "Architected cellular materials: A review on their mechanical properties towards fatigue-tolerant design and fabrication," *Materials Science and Engineering: R: Reports*, vol. 144, p. 100606, Apr. 2021. [Online]. Available: https://www.sciencedirect.com/science/article/pii/S0927796X21000012

[5] G. Comandini, M. Ouisse, V. P. Ting, and F. Scarpa, "Acoustic transmission loss in Hilbert fractal metamaterials," *Scientific Reports*, vol. 13, no. 1, p. 19058, Nov. 2023. [Online]. Available: https://www.nature.com/articles/s41598-023-43646-1

[6] G. Comandini, T. Panzera, A. Celik, A. Gautam, F. Scarpa, M. Azarpeyvand, and V. Ting, "Hilbert Fractal Metamaterials for lightweight sound insulation." e-Forum Acusticum 2020, Dec. 2020, p. 15. [Online]. Available: https://hal.science/hal-03240368

[7] G. Comandini, C. Khodr, V. P. Ting, M. Azarpeyvand, and F. Scarpa, "Sound absorption in Hilbert fractal and coiled acoustic metamaterials," *Applied Physics Letters*, vol. 120, no. 6, p. 061902, Feb. 2022. [Online]. Available: https://doi.org/10.1063/5.0079531

[8] S. A. Naghavi, M. Tamaddon, A. Marghoub, K. Wang, B. B. Babamiri, K. Hazeli, W. Xu, X. Lu, C. Sun, L. Wang, M. Moazen, L. Wang, D. Li, and C. Liu, "Mechanical Characterisation and Numerical Modelling of TPMS-Based Gyroid and Diamond Ti6Al4V Scaffolds for Bone Implants: An Integrated Approach for Translational Consideration," *Bioengineering*, vol. 9, no. 10, p. 504, Oct. 2022. [Online]. Available: https://www.mdpi.com/2306-5354/9/10/504

[9] O. Al-Ketan, D.-W. Lee, R. Rowshan, and R. K. Abu Al-Rub, "Functionally graded and multi-morphology sheet TPMS lattices: Design, manufacturing, and mechanical properties," *Journal of the Mechanical Behavior of Biomedical Materials*, vol. 102, p. 103520, Feb. 2020. [Online]. Available: https://www.sciencedirect.com/science/article/pii/S1751616119312482

[10] L. J. Gibson, "Modelling the mechanical behavior of cellular materials," *Materials Science and Engineering: A*, vol. 110, pp. 1–36, Mar. 1989. [Online]. Available: https://www.sciencedirect.com/science/article/pii/0921509389901548

[11] K. Dutkowski, "Air–Water Two-Phase Frictional Pressure Drop in Minichannels," *Heat Transfer Engineering*, vol. 31, pp. 321–330, Apr. 2010.

[12] P. J. F. Gandy, S. Bardhan, A. L. Mackay, and J. Klinowski, "Nodal surface approximations to the P,G,D and I-WP triply periodic minimal surfaces," *Chemical Physics Letters*, vol. 336, no. 3, pp. 187–195, Mar. 2001. [Online]. Available: https://www.sciencedirect.com/science/article/pii/S0009261400014184

[13] A. Srivastava, "Elastic metamaterials and dynamic homogenization: A review," *International Journal of Smart and Nano Materials*, vol. 6, no. 1, pp. 41–60, Jan. 2015. [Online]. Available: https://doi.org/10.1080/19475411.2015.1017779

[14] E. J. Barbero, *Finite Element Analysis of Composite Materials Using AbaqusTM*, ser. Composite Materials: Design and Analysis. Boca Raton London New York: CRC Press, Taylor & Francis Group, 2013.

[15] J. Somnic and B. W. Jo, "Status and Challenges in Homogenization Methods for Lattice Materials," *Materials*, vol. 15, no. 2, p. 605, Jan. 2022. [Online]. Available: https://www.mdpi.com/1996-1944/15/2/605

[16] W. Yu, "An Introduction to Micromechanics," *Applied Mechanics and Materials*, vol. 828, pp. 3–24, 2016. [Online]. Available: https://www.scientific.net/AMM.828.3

[17] F. J. V. Ribeiro, S. L. M. R. Filho, M. E. Silveira, T. H. Panzera, F. Scarpa, and M. L. P. Tonatto, "A sequential multiscale technique to evaluate the mechanical behaviour of hybrid composites containing carbon fibre and silica microparticles," *Composite Structures*, vol. 314, p. 116977, Jun. 2023. [Online]. Available: https://linkinghub.elsevier.com/retrieve/pii/S0263822323003215

[18] G. Steven, "Homogenization and inverse homogenization for 3D composites of complex architecture," *Engineering Computations*, vol. 23, no. 4, pp. 432–450, Jun. 2006. [Online]. Available: https://www.emerald.com/insight/content/doi/10.1108/02644400610661181/full/html

[19] G. P. Steven, "Homogenization of multicomponent composite orthotropic materials using FEA," *Communications in Numerical Methods in Engineering*, vol. 13, no. 7, pp. 517–531, Jul. 1997. [Online]. Available: https://onlinelibrary.wiley.com/doi/10.1002/(SICI)1099-0887(199707)13:7⟨517::AID-CNM74⟩3.0.CO;2-L

[20] S. L. Omairey, P. D. Dunning, and S. Sriramula, "Development of an ABAQUS plugin tool for periodic RVE homogenisation," *Engineering with Computers*, vol. 35, no. 2, pp. 567–577, Apr. 2019. [Online]. Available: https://doi.org/10.1007/s00366-018-0616-4

[21] W. Tian and L. Qi, "Unified periodic boundary condition for homogenizing the thermo-mechanical properties of composites," *Applied Mathematical Modelling*, vol. 121, pp. 252–269, Sep. 2023. [Online]. Available: https://www.sciencedirect.com/science/article/pii/S0307904X23001762

[22] C. Chatzigeorgiou, B. Piotrowski, Y. Chemisky, P. Laheurte, and F. Meraghni, "Numerical investigation of the effective mechanical properties and local stress distributions of TPMS-based and strut-based lattices for biomedical applications," *Journal of the Mechanical Behavior of Biomedical Materials*, vol. 126, p. 105025, Feb. 2022. [Online]. Available: https://linkinghub.elsevier.com/retrieve/pii/S1751616121006512

[23] A. Pais, J. L. Alves, R. N. Jorge, and J. Belinha, "Multiscale Homogenization Techniques for TPMS Foam Material for Biomedical Structural Applications," *Bioengineering*, vol. 10, no. 5, p. 515, Apr. 2023. [Online]. Available: https://www.mdpi.com/2306-5354/10/5/515

[24] R. Chandra, S. P. Singh, and K. Gupta, "Micromechanical damping models for fiber-reinforced composites: A comparative study," *Composites Part A: Applied Science and Manufacturing*, vol. 33, no. 6, pp. 787–796, 2002.

[25] A. Rezaei, D. Goroz Gómez, F. Gilabert, W. Desmet, and W. Van Paepegem, "Micro-scale finite element simulation of the viscoelastic damping in unidirectional fiber reinforced composites," *Leuven, Belgium: Katholieke Univ Leuven, Dept Werktuigkunde*, pp. 1757–66, 2016.

[26] F. Agnese and F. Scarpa, "Macro-composites with star-shaped inclusions for vibration damping in wind turbine blades," *Composite Structures*, vol. 108, pp. 978–986, Feb. 2014. [Online]. Available: https://linkinghub.elsevier.com/retrieve/pii/S0263822313005436

[27] A. Nateghi, L. Sangiuliano, C. Claeys, E. Deckers, B. Pluymers, and W. Desmet, "Design and experimental validation of a metamaterial solution for improved noise and vibration behavior of pipes," *Journal of Sound and Vibration*, vol. 455, pp. 96–117, Sep. 2019. [Online]. Available: https://www.sciencedirect.com/science/article/pii/S0022460X1930272X

[28] P. Tan, L. Tong, and G. P. Steven, "Behavior of 3D orthogonal woven CFRP composites. Part II. FEA and analytical modeling approaches," *Composites Part A: Applied Science and Manufacturing*, vol. 31, no. 3, pp. 273–281, 2000.

[29] C. Bonatti and D. Mohr, "Smooth-shell metamaterials of cubic symmetry: Anisotropic elasticity, yield strength and specific energy absorption," *Acta Materialia*, vol. 164, pp. 301–321, Feb. 2019. [Online]. Available: https://www.sciencedirect.com/science/article/pii/S1359645418308346

[30] R. Hill, "Elastic properties of reinforced solids: Some theoretical principles," *Journal of the Mechanics and Physics of Solids*, vol. 11, no. 5, pp. 357–372, Sep. 1963. [Online]. Available: https://linkinghub.elsevier.com/retrieve/pii/002250966390036X

[31] V. D. Nguyen, E. Béchet, C. Geuzaine, and L. Noels, "Imposing periodic boundary condition on arbitrary meshes by polynomial interpolation," *Computational Materials Science*, vol. 55, pp. 390–406, Apr. 2012. [Online]. Available: https://www.sciencedirect.com/science/article/pii/S0927025611005866

[32] C. Miehe and A. Koch, "Computational micro-to-macro transitions of discretized microstructures undergoing small strains," *Archive of Applied Mechanics*, vol. 72, no. 4, pp. 300–317, Jul. 2002. [Online]. Available: https://doi.org/10.1007/s00419-002-0212-2

[33] E. E. Ungar and E. M. Kerwin, Jr., "Loss Factors of Viscoelastic Systems in Terms of Energy Concepts," *The Journal of the Acoustical Society of America*, vol. 34, no. 7, pp. 954–957, Jul. 1962. [Online]. Available: https://doi.org/10.1121/1.1918227

[34] R. Shashidhar Reddy and S. Panda, "The energy-based method for effective dynamic properties of viscoelastic composite," *Materials Today: Proceedings*, vol. 18, pp. 4190–4200, 2019. [Online]. Available: https://linkinghub.elsevier.com/retrieve/pii/S221478531932543X

[35] F. Conejos, E. Balmes, B. Tranquart, E. Monteiro, and G. Martin, "Viscoelastic homogenization of 3D woven composites with damping validation in temperature and verification of scale separation," *Composite Structures*, vol. 275, p. 114375, Nov. 2021. [Online]. Available: https://www.sciencedirect.com/science/article/pii/S0263822321008370

[36] D. Garoz, F. A. Gilabert, R. D. B. Sevenois, S. W. F. Spronk, and W. Van Paepegem, "Consistent application of periodic boundary conditions in implicit and explicit finite element simulations of damage in composites," *Composites Part B: Engineering*, vol. 168, pp. 254–266, Jul. 2019. [Online]. Available: https://www.sciencedirect.com/science/article/pii/S1359836818337776

[37] L. J. Gibson, "Cellular Solids," *MRS Bulletin*, vol. 28, no. 4, pp. 270–274, Apr. 2003. [Online]. Available: https://www.cambridge.org/core/journals/mrs-bulletin/article/cellular-solids/D75AD0A311E503438FAC908AA45550B4